Statistical Modeling of Scenario-based indoor WBAN Channels

Badre Youssef, Christophe Roblin, Alain Sibille

Statistical Modeling of Scenario-based indoor WBAN Channels

Badre Youssef, Christophe Roblin, and Alain Sibille, *Senior Member, IEEE*

***Abstract*— This paper presents a parametric statistical path loss model for Wireless Body Area Network (WBAN) communications in the context of a scenario based approach for indoor environments. One of the specificities of WBANs is their numerous sources of variability (subject motion and morphology, antennas, local environment, etc.). We focus here on the influence of the environment, in the case of empty rooms. The model, developed for the first ultra wide band (UWB) sub-band (B = [3.1, 4.8] GHz), takes into account the sizes of the rooms (assumed to be parallelepipedic and empty) and the wall characteristics (via an average reflectivity coefficient). They also involve an elaborate categorization of environments. The following methodology was implemented, in order to avoid time-consuming and complex experimental campaigns while still having a relatively representative and sufficient number of statistical samples: firstly, a simplified ray tracing code enabled a large number of different rooms to be sampled at moderate computational cost; secondly, part of these simulations was supported by anechoic chamber measurements; and thirdly, the simulations were carried out using elaborate experimental designs, based on a categorization of environments and a fairly comprehensive study of building industry data. The parametric path loss models obtained significantly reduce their variance.**

***Index Terms*— WBAN channel, indoor on-body channel, statistical modeling, antennas, experimental design, ray tracing.**

I. Introduction

THE "on-body" WBAN propagation channel, i.e. for which all the radio terminals are placed on a human body, is very special. Firstly, it often has a much larger attenuation than in free space due to propagation mechanisms along or around the human body (consisting of surface waves[1] and/or creeping waves[2]). The close proximity of the terminals to the body generally has a strong influence on the behavior of the antennas and on the propagation mechanisms. Secondly, there are many sources of variability, including those related to the human subject (movement and motion, posture, morphology), to the type and placement of the antennas (distance from the body, orientation and polarization), and to the local propagation environment, especially indoors (room sizes, wall materials, subject location and orientation, etc.). This may explain the complexity of obtaining a generic model for this type of channel and the fact that many propagation channel models have been proposed following different approaches [2] – [9].

In this article, we focus on the "environmental variability"; specifically, we propose a new model of the influence of the characteristics of indoor environments on the path loss (PL) of "on-body" propagation channels. In order to simplify the study while focusing on the environmental contribution related to the room size and wall electromagnetic characteristics, and to extract representative average trend models, the rooms are assumed to be empty. The walls are characterized by an average reflectivity parameter calculated from Fresnel coefficients (which depend on the relative permittivity of the materials $\varepsilon_r = \varepsilon_r' - j\varepsilon_r''$ and on wall thickness). Moreover, this model statistically takes into account the influence of the position and orientation of the subject in the rooms, so we call it an "average model", as opposed to a "local model" which would explicitly takes into account these two parameters.

The contribution of the environment to the propagation channel is itself made up of specular reflections from walls, reflections and diffraction from furniture, as well as the dense multipath component (DMC, including the diffuse component due to the roughness of the surfaces of the walls and furniture, and all of the unresolved multipath components). Since our aim is to identify the main trends in the additional energy contributions brought by the rooms, the parametric ("deterministic") modeling proposed here is limited to specular reflections, which are most often the dominant components.

It should be noted that in publications based on measurements (which therefore take into account all environmental contributions [2]–[11]), the parametric path loss models obtained are site specific (room type and size, furniture, generally unique positioning of the subject, etc.), which is not the aim of our approach.

From our point of view, the environmental contribution has been insufficiently studied and taken into account in existing channel models, both qualitatively and quantitatively. This is probably mainly due to the difficulty and complexity of setting up experiments, which are time consuming and costly, and are sometimes out of reach (as some room sizes are simply not always available).

We therefore adopt an approach based largely on simulation, in part supported by experiment, which allows us to obtain large and statistically representative samples at a moderate cost. The database is obtained for the 1st Ultra Wide Band (UWB) sub-band B = [3.1, 4.8] GHz [12], in the context of the *scenario*

This paper is submitted on July 23, 2023 for review.

B. Youssef and C. Roblin are with the Department of Communication and Electronics, Télécom Paris (Institut Mines-Télécom and LTCI), Palaiseau 91120, France (e-mail: badre.youssef@telecom-paristech.fr).

[1] Waves propagating along a plane or quasi-plane surface (such as an axial path along a cylinder) of a lossy medium, and comprising a "Norton surface wave" (associated with the Sommerfeld pole) and a geometrical-optics field of the first order in r^{-1}. Note that the latter contribution is not always present in "on-body" WBAN radio link, because of the fact that the antennas are generally very close to the body (so that the geometrical-optics field vanishes – as a "space wave") [1]; a slight curvature of the body surface can also play a role here.

[2] Wave that is diffracted around the shadowed surface of a smooth body.

based approach that is considered by many teams to be the most appropriate and accurate [7], [8] and [13]. In this study, five radio links (RL) are considered.

Compared to the state of the art, the novelty of the proposed model lies in the following points: first, a dedicated methodology based on the association of measurements and of electromagnetic (EM) and Ray Tracing (RT) simulations. Second, the specification of a statistically representative Experimental Designs (ED), both qualitatively and quantitatively, which was also an important part of our work. These EDs are constructed from a categorization of environments as realistic as possible (given the information available in the open literature).

The paper is organized as follows: the theoretical and the modeling approaches are presented in section II, Experimental Design (ED) and simulations are described in section III, statistical model and results are exposed in section IV, finally conclusions and perspectives are drawn in section V.

II. Theoretical Approach and Modeling

The present work deals with WBAN communications in the context of the *scenario-based approach*, for five radio links: Hip-to-Chest (H2C), Hip-to-Wrist (H2W), Hip-to-Toes (H2T), Hip-to-Ear (H2E) and Hip-to-Biceps (H2B). This approach has the advantage of not mixing PL results obtained under very different propagation conditions (LOS (Line Of Sight) / NLOS (Non Line Of Sight)) for comparable inter-antenna distances. No fewer than 3000 empty environments classified by categories according to certain geometrical and physical criteria are studied here (cf. section III.A). In order to focus specifically on the environmental effects, the chosen subject is stationary, standing and of average build (165 cm, 50 Kg). Multi-Slot Antennas with a screening BackPlane (MSA-BP [14]) were chosen because of their resilience to body proximity effects.

A. Conventions and notations

The channel *Gain* G_c (resp. *Path Gain PG*) is by definition: $G_c \triangleq |H_c|^2$ (resp. $PG = 10\log G_c$), where H_c is the Channel Transfer Function (CTF, defined by ((2)–(4)). The *Path Loss* is defined as $PL = -PG = -10\log G_c$. The frequency averaging over the band of interest, here B = [3.1, 4.8] GHz, (i.e. over a bandwidth $\Delta f = f_2 - f_1 = 1.7$ GHz) of any quantity $X(f)$, called the "mean value of X", is denoted $\overline{X} \triangleq \frac{1}{\Delta f}\int_{f_1}^{f_2} X(f)df$. The averaging of any quantity $X(f, p_1, p_2, \dots, p_l)$, both in frequency and over some of the parameters $p_n, n \in \{1,2,\dots,l\}$ (i.e. typically a statistical average) is denoted:

$$\begin{aligned}&\bar{X}^{av}\left(p_{k_1}, p_{k_2}, \dots, p_{k_m}\right)\\&= \mathbb{E}\left[\bar{X}\left(p_{l_1}, p_{l_2}, \dots, p_{l_n}\right)\big|_{p_{l_1},p_{l_2},\dots,p_{l_n}\neq p_{k_1},p_{k_2},\dots,p_{k_m}}\right]\\&= \iint \dots \int \bar{X}\left(p_{l_1}, p_{l_2}, \dots, p_{l_n}\right)\big|_{p_{l_1},p_{l_2},\dots,p_{l_n}\neq p_{k_1},p_{k_2},\dots,p_{k_m}} d\mu_{P_m^{\sqsubset}}\\&\sim \langle \bar{X}\left(p_{l_1}, p_{l_2}, \dots, p_{l_n}\right)\rangle_{p_{l_1},p_{l_2},\dots,p_{l_n}\neq p_{k_1},p_{k_2},\dots,p_{k_m}} \qquad (1)\end{aligned}$$

where $P_m = \{p_{k_1}, p_{k_2}, \dots, p_{k_m}\}$ is the subset of the $m \leq l$ random variables (r.v.) over which the average is *not* performed in (1), $P_m^{\sqsubset}$ is its complementary set ($P_m^{\sqsubset} = \{p_{l_1}, p_{l_2}, \dots, p_{l_n}\}\big|_{p_{l_1},p_{l_2},\dots,p_{l_n}\neq p_{k_1},p_{k_2},\dots,p_{k_m}}$ where $n = l - m$), $\mathbb{E}[\cdot]$ is the mathematical expectation, $d\mu_{P_m^{\sqsubset}} = pdf(p_{l_1}, p_{l_2}, \dots, p_{l_n})dp_{l_1}dp_{l_2}\dots dp_{l_n}$ is the joint probability measure of $P_m^{\sqsubset}$ and $\langle\cdot\rangle_{p_1,p_2,\dots,p_l\neq p_{k_1},p_{k_2},\dots,p_{k_m}}$ is the empirical mean (over the set $P_m^{\sqsubset}$). It is assumed that all the corresponding random vectors $\mathbf{P}_m^{\sqsubset}$ admit a joint probability density function (pdf) $pdf(p_{l_1}, p_{l_2}, \dots, p_{l_n})$.

B. Theory and model

The CTF H_c depends on many (quasi-) deterministic parameters and various (mostly random) sources of variability: the considered propagation paths (related to each radio link), the subject's movement and/or posture [10] as well as his morphology [15], the frequency, the antennas [10], [16], [17], and the characteristics of the environment (outdoor/indoor, sizes and materials of the rooms, etc.), as well as the subject's position and orientation, especially in indoor. Since the objective of this article is to model specifically the influence of the environment, as mentioned above, we will consider a "typical" subject (of average build), in standing posture and static position. We will also assume that the antennas are an integral part of the channel. In the following, the term *Path Loss* will be used for this channel (including antennas) in place of "System Loss" recommended by the International Telecommunication Union (ITU-R P.341). The CTF is simply the transmission parameter S_{21} (experimental or simulated) in the reference planes of the transmitting and receiving antennas (located in practice at their connectors):

$$H_c \triangleq S_{21} = S_{21}^{\mathrm{On}} + S_{21}^{\mathrm{Env}} \qquad (2)$$

Here we distinguish the "on-body" contribution S_{21}^{On} (of the "paths" along, around or in the immediate vicinity of the body) from that of the environment S_{21}^{Env}, including the effects of its more or less close scatterers (specular reflections, diffractions, and the so-called "dense" component, including the diffuse radiation due to the roughness of the walls and, more generally, all of the unresolved multipath components).

Since the goal of this paper is to identify the main trends of a "central model" (in the sense that it depends only on the characteristics of the environment and not on the position or orientation of the subject), of moderate complexity, we limit ourselves to the contribution of specular reflections in empty parallelepipedic rooms. By further restricting to the four reflections on the side walls ($S_{21}^{(p)}\big|_{p=1,\dots,4}$) – assuming that they constitute the dominant part of the environmental contribution – it comes:

$$S_{21}^{\mathrm{Env}} = \sum_{p=1}^{4} S_{21}^{(p)} + \Delta S_{21}^{\mathrm{Env}} \qquad (3)$$

where $\Delta S_{21}^{\mathrm{Env}} = S_{21}^{\mathrm{gnd}} + S_{21}^{\mathrm{ceil}} + S_{21}^{\mathrm{HO}}$ represents the other environmental contributions, i.e., direct specular reflections from the floor and ceiling (which depend only on their characteristics and the "height" of the antennas or ceiling, but do not depend on any other characteristics of the room – especially its size – nor on the position or orientation of the

subject), as well as all higher order interactions (S_{21}^{HO}).

We can show that $S_{21}^{(p)}$ follows the form:

$$S_{21}^{(p)} = \kappa(f,\psi)\frac{e^{-jkd_p}}{d_p} \sim \kappa_0(f, D_p^{(0)}, \psi)\frac{e^{-j2kD_p^{(0)}}}{D_p^{(0)}} \quad (4)$$

where d_p is the p-th path length, $D_p^{(0)}$ is the distance of the subject's "Macro-position" center (Mp, Figure 2) to the p-th wall (expressed in (6) and (7)), k is the wave number and ψ the subject's orientation (Figure 2). κ is a proportionality coefficient that depends on the Antenna Transfer Functions (ATF) $\boldsymbol{\mathcal{H}}$ [18] (worn by the subject), Fresnel reflection coefficients and the geometry of the radio link under consideration (which depends on the stature of the subject), and is a fairly smooth function of f. Assuming that the HN segment linking the nodes ("Hip-to-Node") intersects the subject's axis of rotation at C (Figure 1), and noting $a_{1,2}$ the lengths of the HC and CN segments, we can show, after a few somewhat cumbersome but elementary calculations, that:

$$d_p = \frac{2D_p^{(0)}}{\cos\alpha_p} + (a_1 - a_2)\xi(\psi) = 2D_p^{(0)}\left\{1 + \mathcal{O}\left(\frac{|a_1 - a_2|}{D_p^{(0)}}\right) + \mathcal{O}\left(\frac{a^2}{\left(D_p^{(0)}\right)^2}\right)\right\} \quad (5)$$

for $|a_1 - a_2| < a \ll D_p^{(0)}$ and where $\xi(\psi)$ verifies $|\xi(\psi)| \leq 1$ and $\xi(0) = 0$. Even though this approximation may be rather rough for some scenarios[3], it proves to give good results (section IV). Hence, the second expression of (4) is an approximation considering that $d_p \cong 2 \cdot D_p^{(0)}$ where most often κ_0 depends only weakly on $D_p^{(0)}$. Eventually, the channel gain G_c will be averaged over the subject's orientation parameter ψ in subsequent processing dedicated to the extraction of the average model.

$$D_1^{(0)} = \frac{L}{2} - x_{\mathrm{M}}, \qquad D_2^{(0)} = \frac{W}{2} - y_{\mathrm{M}} \quad (6)$$

$$D_3^{(0)} = \frac{L}{2} + x_{\mathrm{M}}, \qquad D_4^{(0)} = \frac{W}{2} + y_{\mathrm{M}} \quad (7)$$

where $(x_{\mathrm{M}}, y_{\mathrm{M}})$ are the coordinates of any subject's Mp with: $(x_{\mathrm{M}}, y_{\mathrm{M}}) \in \left[-\frac{L}{2} + d_m, \frac{L}{2} - d_m\right] \times \left[-\frac{W}{2} + d_m, \frac{W}{2} - d_m\right]$, and d_m the subject's half shoulder width.

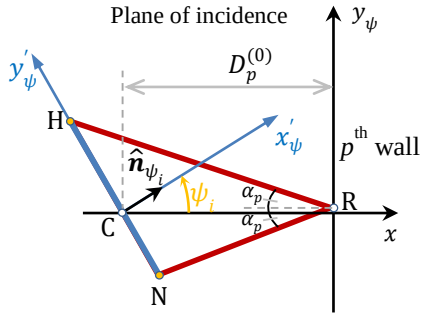

ψ_i is the subject's rotation angle, seen in the plane of incidence (which is not necessarily horizontal).

$\psi_i \sim \psi$ as defined in Figure 2.

Figure 1. "Hip-to-Node" geometry in the plane of incidence.

[3] when the subject is close to a wall (which is therefore statistically in the minority), notably for the H2C link; however, it should be noted that for the latter, the relative contribution of the environment is the lowest.

Consequently, posing $\Delta S_{21} \triangleq S_{21}^{\mathrm{On}} + \Delta S_{21}^{\mathrm{Env}}$, the channel gain G_c is given by:

$$G_c = \left|\Delta S_{21} + \sum_{p=1}^{4} S_{21}^{(p)}\right|^2 = |\Delta S_{21}|^2 + \sum_{p=1}^{4}\left|S_{21}^{(p)}\right|^2 + 2\Re e\left\{\Delta S_{21}^* \sum_{p=1}^{4} S_{21}^{(p)}\right\} + \sum_{p=1}^{4}\sum_{\substack{q=1 \\ q\neq p}}^{4} S_{21}^{(p)} S_{21}^{(q)^*} \quad (8)$$

For a given macro-position, the exact positioning of the subject in the room also depends on its orientation ψ and on the micro-positioning µp. The latter involves small-scale spatial sampling along a segment oriented at the angle ψ on either side of the Mp (cf. sketch of the µp in Figure 2 insert). This micro-positioning will later be used to average out small-scale fading.

In practice, for each Mp, a random angle ψ_0 is drawn uniformly over [0,2π[, and 15 other values of ψ ($\psi_n = \psi_0 + n\Delta\psi$, $n = 1, \ldots, 15$) are chosen by successive shifts of $\Delta\psi = \frac{\pi}{8}$ rad. For each value of ψ, 6 µp are sampled (at sub-wavelength scale) on either side of the Mp with a step $\delta\mu = \frac{\lambda_{min}}{2} = \frac{c}{2f_{max}} \approx$ 3 cm (so that the actual distance to the p-th wall ($p = 1, \ldots, 4$) is $D_{p\mu}^{(0)} = D_p^{(0)} + (\frac{7}{2} - \mu)\delta\mu \sin[\psi - p\frac{\pi}{2}]$, with $\mu = 1, \ldots, 6$,).

Therefore, *EC* referring to "Environment Category" (defined in section III.A), it comes:

$$\bar{G}_c^{av}(RL, EC, L, W) = \langle \bar{G}_c(RL, L, W, x_{Mp}, y_{Mp}, \mu, \psi)\rangle_{\mu, x_{Mp}, y_{Mp}, \psi} \quad (9)$$

$$\bar{G}_c^{av}(RL, EC, L, W) = \langle\overline{|\Delta S_{21}|^2}\rangle + \sum_{p=1}^{4}\langle\overline{\left|S_{21}^{(p)}\right|^2}\rangle + 2\,\langle\overline{\Re e\left\{\Delta S_{21}^* \sum_{p=1}^{4} S_{21}^{(p)}\right\}}\rangle + \sum_{p=1}^{4}\sum_{\substack{q=1 \\ q\neq p}}^{4}\langle\overline{S_{21}^{(p)} S_{21}^{(q)^*}}\rangle \quad (10)$$

It can be shown that, statistically, the first two terms are generally dominant. Indeed, the terms containing $S_{21}^{(p)} \propto e^{-jkd_p}$ or $S_{21}^{(p)} S_{21}^{(q)^*} \propto e^{-jk(d_p - d_q)}$ are functions that oscillate rapidly in frequency (unless $|d_p - d_q| \ll \lambda_{min}$ for the last, which happens statistically only rarely if $q \neq p$. Subsequently, summing over the frequency band B tends to result in a vanishing integral. This effect is even more pronounced when small-scale spatial averaging is also performed.

Since the macro-positions are assumed to be uniformly distributed over the "accessible" area of the rooms (i.e. the rectangle $\left[-\frac{L}{2} + d_m, \frac{L}{2} - d_m\right] \times \left[-\frac{W}{2} + d_m, \frac{W}{2} - d_m\right]$), the mean average gain $\bar{G}_c^{av}$ – given by (10) – is calculated as follows (note that in the following (x, y) are the "exact" coordinates of the subject, taking into account the micro-positioning):

$$\bar{G}_c^{av}(RL, EC, L, W) = \frac{1}{(L-2d_m)(W-2d_m)}\frac{1}{\Delta f}\int_{-\frac{L}{2}+d_m}^{\frac{L}{2}-d_m}\int_{-\frac{W}{2}+d_m}^{\frac{W}{2}-d_m}\cdots \cdots \int_{f_1}^{f_2}\langle G_c(RL, f, L, W, x, y, \mu, \psi)\rangle_{\mu,\psi} dx dy df \quad (11)$$

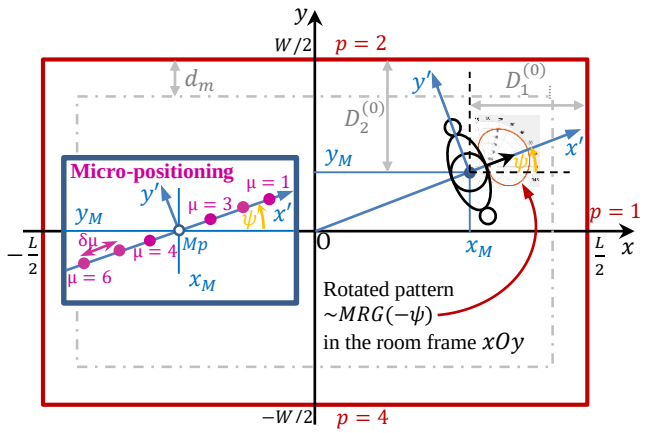

Figure 2. Room geometry and subject position (top view).

In this integral, the integrand of (11) contains terms depending on x and/or y of the form (taking into account the approximations explained above) $\frac{1}{D_p^{(0)}}$ or $\frac{1}{D_p^{(0)}D_q^{(0)}}$, i.e.:

$$\frac{1}{\left(\frac{L}{2}\pm x\right)^2},\frac{1}{\left(\frac{W}{2}\pm y\right)^2},\frac{1}{\frac{L}{2}\pm x},\frac{1}{\frac{W}{2}\pm y},\frac{1}{\left(\frac{L}{2}\pm x\right)\left(\frac{W}{2}\pm y\right)},\frac{1}{\frac{L^2}{4}-x^2},\frac{1}{\frac{W^2}{4}-y^2} \quad (12)$$

which lead, after integration, to the following terms:

$$\frac{1}{L-d_m},\frac{1}{W-d_m},\frac{\ln(L/d_m-1)}{L-2d_m},\frac{\ln(W/d_m-1)}{W-2d_m},$$
$$\frac{\ln(L/d_m-1)\ln(W/d_m-1)}{(L-2d_m)(W-2d_m)},\frac{\ln(L/d_m-1)}{L(L-2d_m)},\frac{\ln(W/d_m-1)}{W(W-2d_m)} \quad (13)$$

On the other hand, the channel gain of each of the four dominant paths depends on the lateral walls reflectivity, i.e. on their (multilayer) Fresnel reflection coefficients $r_{\perp,||}$ for Transverse Electric (resp. Magnetic) polarized incident waves, recalled here for convenience (for a wall of thickness d) :

$$r_{\perp,||} = r_{\mathrm{TE,TM}} = \frac{1-e^{-2jk_pd}}{1-\Gamma_{||,\perp}^2 e^{-2jk_pd}}\Gamma_{\perp,||} \quad (14)$$

with $\Gamma_{\perp,||}$ the Fresnel coefficients of an indefinite plane interface of relative permittivity $\varepsilon_r = \varepsilon_r' - \varepsilon_r''$ and $k_p = 2\pi f\sqrt{\varepsilon_r}/c$ the wavenumber in the p-th wall. Furthermore, we assume that the two polarizations of the specular reflections are equiprobable, and that the incidence angle θ_i (in the plane of incidence) is uniformly distributed over $[0, \Delta\theta_i]$ where $\Delta\theta_i < \pi/2$ is a maximal value to be set from the geometry. Although these assumptions are rather rough, their merit is that they simplify the modeling very significantly, while turning out to give very good results when used for modeling the Power Delay Profile and the Delay Spread of the indoor propagation channel in empty homogeneous rooms [19] and [20]. The statistical fits of the models obtained in section IV are also satisfactory, which has led us to retain these simple assumptions.

Finally, the walls being different and possibly inhomogeneous, we use an *effective* reflection coefficient, computed as a mean coefficient $\bar{r}_{av}$, averaged over both polarizations as abovementioned, and over each homogeneous part of the vertical walls, weighted by their respective area, i.e.:

$$\bar{r}^{av} = \sqrt{\bar{R}^{av}} = \sqrt{\frac{1}{2}\left(\bar{R}_{\perp}^{av} + \bar{R}_{||}^{av}\right)} \quad (15)$$

where $\bar{R}_{\perp,||}^{av}$ are the mean power reflection coefficients, averaged overs the walls, i.e.:

$$\bar{R}_{\perp,||}^{av} = \frac{1}{A_w}\sum_{p=1}^{4}\sum_{n=1}^{n_p} A_w^{(p,n)}\frac{1}{\Delta\theta_i}\int_0^{\Delta\theta_i}\bar{R}_{\perp,||}^{(p,n)}(\theta_i)d\theta_i \quad (16)$$

where $A_w = \sum_{p=1}^{4}\sum_{n=1}^{n_p} A_w^{(p,n)}$ is the total area of the vertical walls, each comprising n_p homogeneous parts of area $A_w^{(p,n)}$, and $\bar{R}_{\perp,||}^{(p,n)}(\theta_i) = \frac{1}{\Delta f}\int_{f_1}^{f_2}\left|r_{\perp,||}^{(p,n)}(\theta_i, f)\right|^2 df$.

The input parameters of the model must be chosen to cover all the terms in (13) resulting from the development (10) – after integration (11) over all the subject's positions – while minimizing their number, as well as the complexity of the multilinear regression model (18) (i.e. the number of its coefficients). Note that the appearance of a Fresnel coefficient in field $\bar{r}_{av}$ or power $\bar{R}^{av}$ depends on whether the abovementioned terms come from a linear or quadratic contribution in $S_{21}^{(p)}$ in (10). These constraints lead to the following choice (to represent all the terms in (13) while minimizing the number of product terms in (18)):

$$x_1 = \frac{\bar{R}^{av}}{L-d_m},\ x_2 = \frac{\bar{R}^{av}}{W-d_m},\ x_3 = \bar{r}^{av}\frac{\ln(L/d_m-1)}{L-d_m},$$
$$x_4 = \bar{r}^{av}\frac{\ln(W/d_m-1)}{W-d_m}, x_5 = \frac{\bar{r}^{av}}{L}, x_6 = \frac{\bar{r}^{av}}{W} \quad (17)$$

The multi-linear regression parametric models are therefore written:

$$\hat{\bar{G}}_c^{av}(RL, EC, L, W) = \alpha_0 + \sum_{n=1}^{4}\alpha_n x_n + \alpha_{34}x_3x_4 + \alpha_{35}x_3x_5 + \alpha_{46}x_4x_6 \quad (18)$$

where $(\alpha_0, \ldots, \alpha_n, \{\alpha_{mn}\}) = \boldsymbol{\alpha}(RL, EC)$ are the coefficients of the parametric models, and $\delta\bar{G}_c^{av} = \bar{G}_c^{av} - \hat{\bar{G}}_c^{av}$ are zero-mean r.v. representing the model errors (or *residuals*)[4].

III. Experimental Design and Simulations

The development of any statistical model is based on the collection of data in one or more statistical samples. Experimental Design consists in defining these samples so that they are sufficiently representative (statistically), while at the same time aiming to minimize the cost of their collection and/or subsequent processing. An experimental design therefore consists in choosing the random input parameters, their statistics (ranges of variation, distributions, possible dependencies, etc.), as well as the method(s) or algorithm(s) used to generate the samples. Several ED based on a categorization of environment types and the Latin Hypercube Sampling (LHS) technique [21] were established.

A. Categorization of Environments

The environment/room categorization developed in this work is based on an analysis of the specialized real estate literature (of the French building stocks), as well as the

[4] Note that more generally, the α's also depend on the worn antennas (typically through their mean efficiency as the averaging of G_c over ψ and f tends to "omnidirectionalize" their mean realized gain patterns), as well as on the morphology and posture of the subject.

regulatory standards and recommendations of the building sector, according to the following criteria: size of the premises, room "aspect ratio" (L/W), wall thickness [22]–[24], as well as wall materials [25]–[28]. We identified two main categories: residential and office, which we subdivided into subclasses.

TABLE I
STATISTICAL PARAMETERS OF ENVIRONMENTS SIZES

Env.	**Residential** [min, max], mode, median (m)		
	Width	**Length**	**Height**
Bedroom	[3, 4], 3.3, 3.6	[3.1, 4.8], 3.7, 3.9	2.4
Living room	[2.8, 4], 3.2, 3.3	[5, 10], 6.7, 7.1	2.4
Env.	**Office** [min, max], mode, median (m)		
	Width	**Length**	**Height**
Office	[2.2, 3.4], 2.6, 2.7	[4, 6], 4.7, 4.8	2.7
Meeting room	[2.2, 5], 3.1, 3.3	[4.2, 12], 6.8, 7.4	2.7
Classroom	[5, 8.5], 6.2, 6.5	[6, 11.5], 7.9, 8.3	2.7
Corridor	[0.9, 4], 1.9, 2.2	[2.6, 60], 21.7, 26.2	2.7

TABLE II
WALL THICKNESSES

Wall		**Material**	**Thickness (cm)** [min, max], mode, median
Wall	Bearing wall	Hollow brick	[15, 30], 20, 20
		Reinforced concrete[1]	[20, 35], 23, 25
		Cinder Block	[15, 35], 20, 22
	Bulkhead	Plaster	[15, 30]
		Brick[2]	[5, 15]
	Glass Single glazing		[0.4, 0.6]
	Glass Double glazing		[0.4 1.2 0.4] [0.4 1.6 0.4]
	Wood		[3, 4]
Ceiling	Reinforced concrete		[12, 20], 15, 15
Floor	Reinforced concrete		L/25 with a max. of 40 cm

1. An air gap, two thirds of the total thickness, is considered.
2. If thickness > 10cm an air gap in the middle of one third of the thickness is taken into account.

TABLE III
WALLS MATERIALS RELATIVE PERMITTIVITY

Material	**Complex Relative Permittivity** [min, max], mode, median	
	ε_r'	ε_r''
Brick	[3, 6], 3.8, 3.8	[0.02, 0.6]
Reinforced concrete	[3, 9], 5.2, 5.8	[0.1, 1.5]
Cinder Block	[2.5, 7], 4, 4.5	[0.1, 1.5]
Plaster	[1.9, 2.9]	0.14
Glass	[4, 7], 6, 6	0.1
Wood	[1.2, 6] 2, 3	0.1

For the first category, we selected the bedroom and living room, and for the second, the office, meeting room, classroom and corridor. Wall characteristics (thickness and materials) are summarized in Tables II and III. For the reinforced concrete, a conductivity $\sigma = 0.1\ \mathrm{S/m}$ is also considered.

The variability of the considered parameters (aiming for greater representativeness) is significant compared to other studies in which the environments were considered homogeneous with limited variability in room size and subject location (usually single) [3], [6], [8] – [11] and [16].

B. Experimental Design and simulations

1) Input Parameters

The input parameters of the EDs are the room sizes (L, W, h), wall characteristics (materials and thicknesses) related to the subclass and the location and orientation of the subject.

As the objective of this work is to develop "average" statistical parametric models, and as the PL depends more or less significantly on the position and orientation of the subject (depending on the RL considered), these "hidden parameters" do not appear explicitly in the model structure but their statistical contribution is nevertheless taken into account on average, since the channel gain will later be averaged over these parameters, as was presented in section II.

The statistics of the input variables are based on the values of four parameters[5] (the extreme values, x_{min} and x_{max}, as well as the median and mean values m_x and μ_x), which are in part accessible in the specialized literature (statistics of the French building stock, laws and regulatory constraints of the building sector, publications on the permittivity of building materials). Indeed, the statistics of the building sector are often fragmented, and limited to simple data such as moments of order 1 (average and/or median). It is much more difficult to obtain information on the variability of room sizes and their statistics (especially their distributions), for which there is no accessible literature to the best of the authors' knowledge. Thus we also relied on ITU models in some cases [29]. Regarding the thickness of the walls, we rely on construction standards. Gathering sufficient information on material permittivity statistics has also proven difficult. Our estimates are based on cross-referencing various publications and sources of information. This is why we also rely on "common sense" and real life experience, as well as on the "principle of parsimony" ("Occam's razor"). Accordingly, simple and sufficiently versatile distributions are here chosen, with bounded support for obvious practical reasons, and whose parameters can be easily expressed in terms of the four (or two) parameters mentioned above. The marginal pdf of the input variables listed in Table I-Table III are chosen as follows: for variables depending only on the two extreme parameters (x_{min} and x_{max}) we assume that a uniform distribution $\mathcal{U}([x_{min}, x_{max}])$ is adequate. For 4-parameter variables, we use the beta distribution $\mathcal{B}(r, s, x_{min}, x_{max})$, because it is quite versatile, has bounded support, can be symmetric or not, while skewness and kurtosis can be expressed in closed-form as a

[5] in some cases, on 2 parameters only (the extreme values), especially when the interval is quite small.

function of its parameters. The latter can also be easily expressed as a function of the four aforementioned parameters x_{min}, x_{max}, m_x and μ_x (Table I-Table III):

$$X \sim \mathcal{B}(r, s, x_{min}, x_{max}), \quad r > 0, \quad s > 0 \tag{19}$$

$$f_X(x) = \frac{(x - x_{min})^{r-1}(x_{max} - x)^{s-1}}{(x_{max} - x_{min})^{r+s-1} B(r,s)} \mathbb{1}_{[x_{min}, x_{max}]}(x) \tag{20}$$

with $B(r,s) = \Gamma(r)\Gamma(s)/\Gamma(r+s)$ the Beta function (and Γ the Gamma function) [30] and $\mathbb{1}_{[a,b]}$ is the indicator function of the segment $[a, b]$.

Categorizing environments requires to enforce certain constraints, not only on the size of the rooms but also on their "aspect ratio" (L/W)[6]. In other words, for each subclass, the variables *L* and *W* are not independent. In order to model these possible dependencies, which are not necessarily linear, we choose to use copulas. In probability theory and statistics, copulas are mathematical functions that can be used to describe or model the dependence (not necessarily linear) between random variables. In particular, Sklar's theorem states that, under certain conditions, any multivariate joint distribution can be written in terms of univariate marginal distribution functions and a copula that describes the dependence structure between the variables. In other words, among many other interesting features and properties, the use of copulas is an elegant and efficient way to generate statistical samples of a random vector which components are dependent. For this specific purpose, only the marginals and the copula need to be known or estimated *separately* (it is not necessary to know the joint pdf, which can be deduced from them). Note that there are many families of parametric copulas, whose parameters control the strength of the dependence [31].

Concerning materials, for each subclass, the walls considered are inhomogeneous (refer to Table II and Table III). All the premises have a wall with a (wooden) door. Depending on the subclass, a wall with a window is also taken into account, either for the whole sample or for a proportion of it (office, meeting room, corridor office). The glazed area of walls is considered to be proportional to the floor area (around 1/5 according to the room [32]).

The subject turning on himself at each macro-position, is represented by his "footprint", i.e. a disk with the diameter of his shoulder width ($d_{Mp} = 2d_m = 50$ cm here). In order to avoid overlap of these disks, spatial sampling was performed by combining the LHS technique with a *maximin* algorithm. Moreover, in order to reduce as much as possible the computational cost, hence the sample size, the density of Mp (D_{Mp} in Mp/m^2) was significantly reduced from the maximal room paving (without overlap) which most often corresponds to a triangular mesh of density $D_{Mp} \approx 4$ Mp/m^2 (covering $\approx$ 90.7 % of the floor area). An "optimal" density of about $D_{Mp,opt} = 1$ Mp/m^2 (i.e. a reduction by a factor of 4) proved to be a good compromise between computational cost and statistical representativeness. This was established by performing Kolmogorov-Smirnov (KS) tests on the mean average Path Loss $\overline{PL}^{av} = -10 \log \bar{G}_c^{av}$ for a few representative environments and three clearly different RLs.

[6] For example, the bedrooms are rather square while the corridors are obviously elongated.

2) *Ray Tracing Simulations*

A simplified RT code (based on image theory) considering specular reflections only (up to order 3) has been developed (under Matlab®). The simplifying assumptions of the proposed modeling are therefore the following: the rooms are empty and the walls are smooth, so that the diffraction on the furniture (and on the irregularities of the walls) and the diffuse scattering are neglected. This tool allows to sample with great flexibility a large number of environments and subject positions (and orientations) within each room. For this study, this allowed us to consider a total of 3000 rooms (500 per environment subclass).

The simulation approach using a RT code that considers only specular reflections was supported by a comparison with experimental PL measurements carried out in 4 classrooms [16] considering 3 radio links (H2C, H2W and H2T). The RT tool was calibrated for the unknown parameters (wall permittivities and thicknesses). The choice of these parameters was of course made within typical ranges published in the literature.

TABLE IV
ROOM SIZES

Room	*L* (m)	*W* (m)	*h* (m)	Materials considered
1	8.56	8.16	3.75	brick, cinder block and glass
2	8.13	6.51	3.60	brick, cinder block and glass
3	5.93	4.80	3.60	brick, cinder block and glass
4	5.10	5.10	2.47	Metal and glass

The comparison of the mean average $\overline{PL}^{av}$ is shown in Figure 3 with $\overline{PL}^{av} = 10\log(1/\bar{G}_c^{av})$.

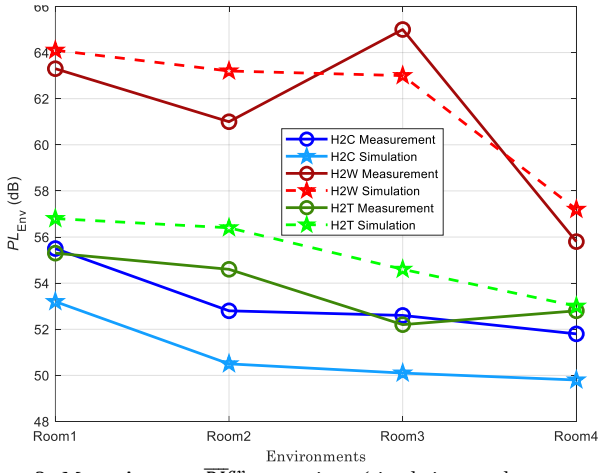

Figure 3. Mean Average $\overline{PL}^{av}$ comparison (simulations and measurements results).

The deviations observed are typically of the order of 2 dB, which, given the strong approximations and simplifications made, seems satisfactory and consistent, and therefore supports

the approach adopted.

Some studies have used RT tools that are more precise the higher the frequency (of course, the higher the frequency, the more justified the use of this type of asymptotic approach) [33]. Even with a simplified approach like the one presented here, and in lower frequency domains, we have noted that the results obtained with the RT algorithm were satisfactory [34].

3) Antennas and on-body component

The on-body contribution (S_{21}^{On}) and the ATF in transmission $\boldsymbol{\mathcal{H}}$ ($\boldsymbol{\mathcal{H}}(f,\theta,\varphi) = re^{jkr}\sqrt{\frac{4\pi}{\eta_0}}\cdot\frac{\mathbf{E}^{\infty}(f,\mathbf{r})}{a_1(f)}$) are obtained from Electromagnetic simulations with CST Studio Suite®, where a_1 is the incident wave at antenna port, $\mathbf{E}^{\infty}$ the radiated Far-Field, η_0 the free space impedance, and (θ,φ) the elevation and azimuth angles [17]. The subject, of average build, is modeled by an anthropomorphic inhomogeneous phantom ("*Louis*") of the IT'IS Foundation Virtual Population suite [35].

These simulations were previously validated by comparison with measurements performed in an anechoic chamber with a homogeneous whole body phantom ("Kevin") whose morphology is close to that of Louis [16]. A "homogenized" version of Louis, with the same permittivity $\varepsilon_r(f)$ as Kevin, was used as an "intermediate model" to compare the simulated and measured radiation patterns.

For the on-body contribution, the adequacy of the simulations was evaluated by comparison with anechoic chamber measurements of the mean PL: $\overline{PL}^{\mathrm{On}}(RL) = -10\log\overline{\left|S_{21}^{\mathrm{On}}(RL)\right|^2}$. The differences between the results, presented in Table V, are generally of the order of 1 dB (~2 dB between the measurement and "Louis homogeneous" for the H2T RL).

TABLE V
MEAN ON-BODY PL – CST SIMULATIONS VS MEASUREMENTS

PL (dB)	H2C	H2W	H2T	H2B	H2E
Simulations – Louis Inhomogeneous	47.3	70.7	55.0	70.0	67.7
Simulations – Louis Homogeneous	48.1	69.3	57.2	71.0	66.6
Measurements – Kevin	49.1	69.5	57.8	72.2	68.5

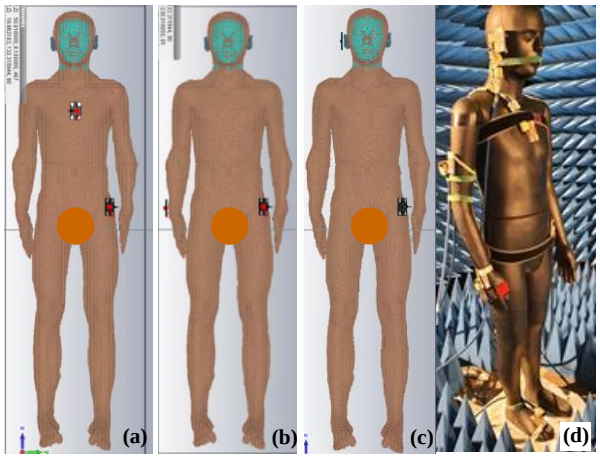

Figure 4. (a) H2C, (b) H2W and (c) H2E simulated with CST with "Louis"; (d) measurement of 5 RL on *Kevin* in anechoic chamber.

Similarly, for the antenna patterns, an example of azimuthal cuts of the total Mean Realized Gain (including both polarizations, defined as $MRG = \frac{1}{\Delta f}\int_{f_{min}}^{f_{max}}\|\boldsymbol{\mathcal{H}}(f)\|^2\,df$ in [17] and [34]) is shown for the chest and wrist antennas in Figure 6.

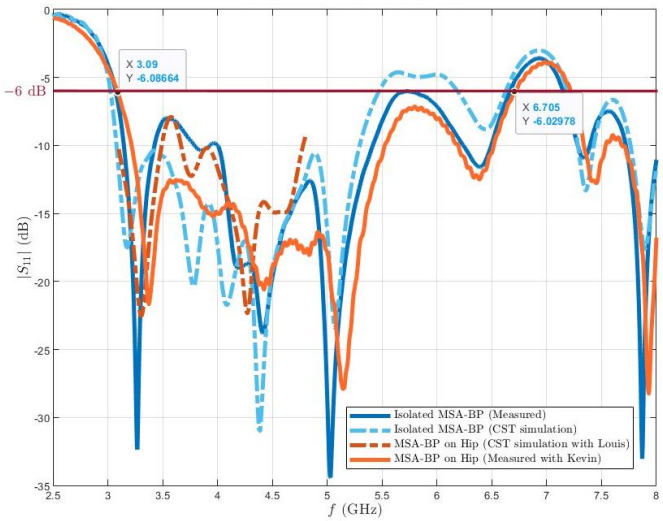

Figure 5 Reflection coefficient of the MSA-BP (isolated and on Hip).

The MRG (over B = [3.1, 4.8] GHz) cuts presented in Figure 6 are close to the azimuth (i.e. elevation angle $\theta \sim 90°$) because the rays reflected only once over the vertical walls are most often close to the azimuthal plane (as statistically the subject is far from them).

Given the satisfactory agreement between simulations and measurements in the horizontal plane, especially in the particularly important main lobe, we subsequently rely on simulations for elevation angles where on-body antenna patterns are intrinsically difficult to measure (for obvious practical reasons).

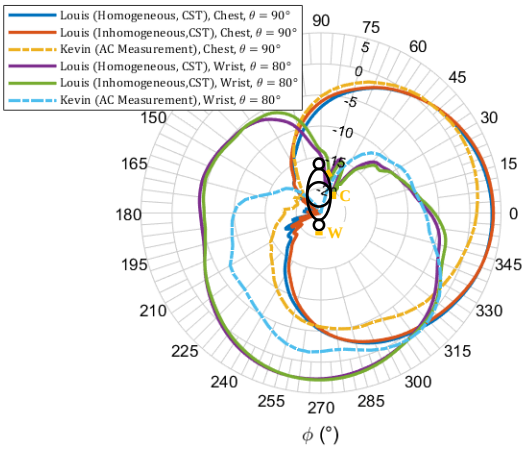

Figure 6. Simulated (CST) and measured MRG azimuthal patterns for MSA-BP on Chest and Wrist.

IV. STATISTICAL MODEL AND RESULTS

A. Model validation with a simplified case

The structure of the model (i.e. the relevance of the explicative variables x_n of (17)) was first validated on a "test sample" of reduced size (100 realizations) with a simplified ED. In this test, the six walls are homogeneous and have the same

characteristics (permittivity and thickness), resulting in a reduced variability, and the size statistics roughly match those of the classroom and office subclasses. Nevertheless, the excursion of variability in this test case remains greater than what has been published in the literature to date.

According to common practice in statistics, the goodness of fit of the models is assessed by classical performance indicators, which are the coefficient of determination R^2 on one hand and the ratio χ between the primary and residual variances, on the other. The former is defined as:

$$R^2 = 1 - \frac{\sum_{i=1}^{n}(y_i - \hat{y}_i)^2}{\sum_{i=1}^{n}(y_i - \langle y \rangle)^2} \quad (21)$$

where n is the number of measurements, y_i the value of i^{th} measurement, $\hat{y}_i$ the corresponding predicted value and $\langle y \rangle$ the average of the measurements, and the latter as:

$$\chi = \frac{\sigma^2_{\bar{G}_c^{av}}}{\sigma^2_{\delta\bar{G}_c^{av}}} \quad (22)$$

The differences between the model extracted for this test and the data are small, as can be seen from the high R^2 values (close to 1). Parametric modeling also significantly reduces the variance (χ ranging between 31.6 and 385.5) as referred in Table VI and illustrated in Figure 7 for the H2C RL. The trends for the other links are similar.

It is interesting to note that this error appears as a zero-mean Gaussian random variable (r.v.), contrary to the initial dataset, which simplifies the overall modeling. This analysis therefore validates the structure of the model, highlighting the relevance of the explicative variables derived from the modeling.

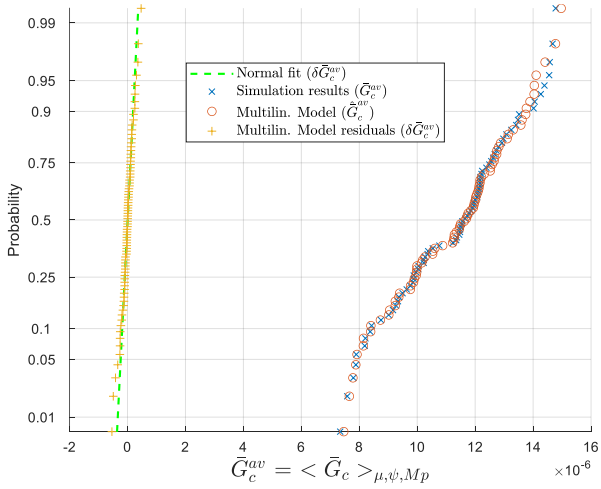

Figure 7. Probability plot of $\bar{G}_c^{av}$, $\hat{\bar{G}}_c^{av}$ and residuals. Test sample (H2C).

TABLE VI
R^2 AND χ FOR THE "TEST SAMPLE"

RL	H2C	H2W	H2T	H2E	H2B
R^2	0.991	0.993	0.968	0.997	0.996
χ	110.0	147.1	31.6	385.5	253.8

B. *Statistical Models*

1) *Extraction of regression models*

The results presented here are the mean average gain $\bar{G}_c^{av}$ and the multilinear regression models $\hat{\bar{G}}_c^{av}$ for each environment and RL presented above. To assess the representativeness of the results obtained, the performance indicators described previously (R^2 and χ) are used. In addition, a cross-validation technique is applied to each model to test its robustness and ensure that there are no overfitting issues.

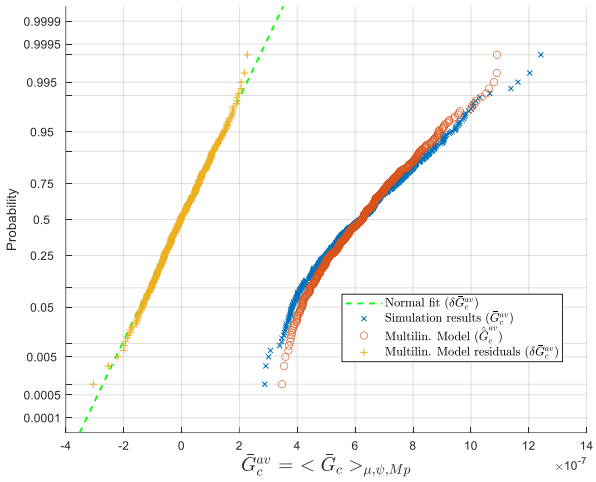

Figure 8. Typical case. Probability plot of $\bar{G}_c^{av}$, $\hat{\bar{G}}_c^{av}$ and residuals. Meeting room (H2W).

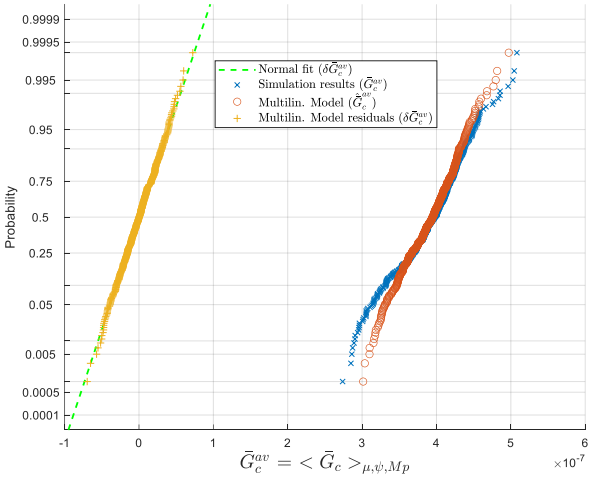

Figure 9. Worst case. Probability plot of $\bar{G}_c^{av}$, $\hat{\bar{G}}_c^{av}$ and residuals Classroom (H2B).

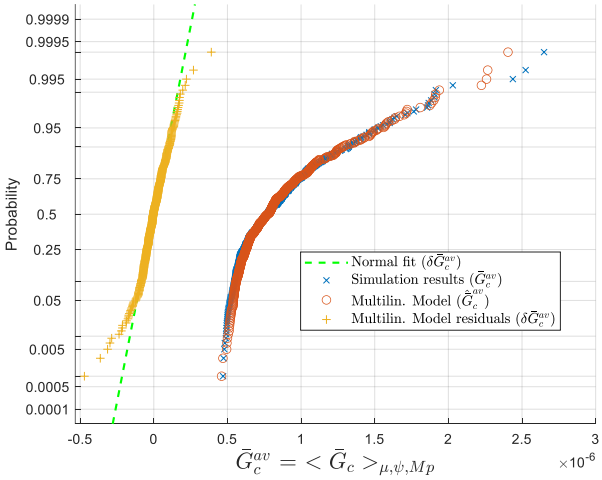

Figure 10. Best case. Probability plot of $\bar{G}_c^{av}$, $\hat{\bar{G}}_c^{av}$ and residuals. Corridor Office (H2E).

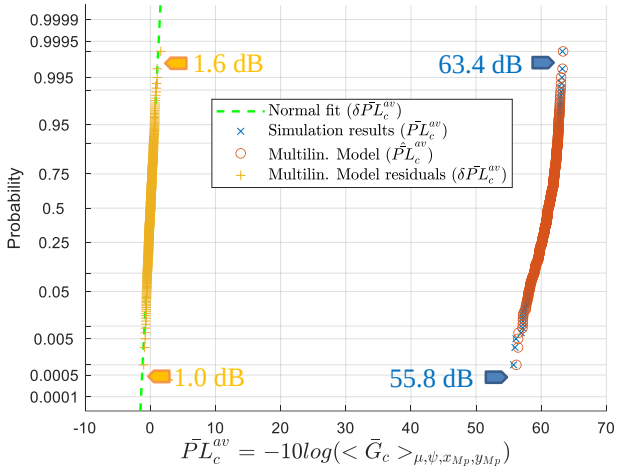

Figure 11. Example of probability plot of $\overline{PL}_c^{av}$, $\widehat{\overline{PL}}_c^{av}$ and residuals in dB. Corridor Office (H2E).

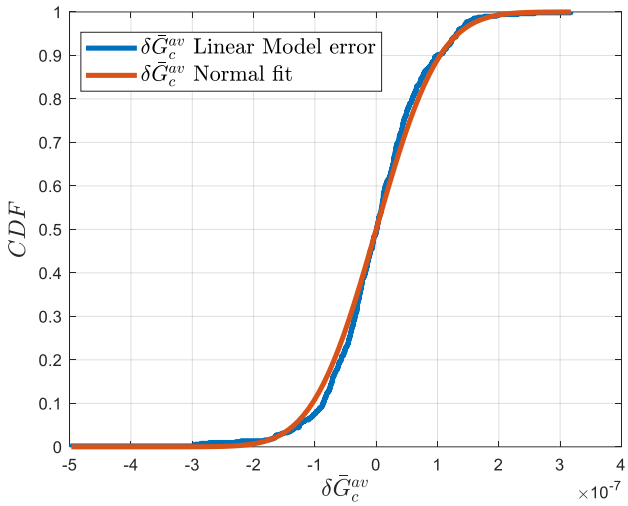

Figure 12. CDF residuals $\delta\bar{G}_c^{av}$. Corridor Office (H2E).

The performance indicators have been calculated in Table VII and Table VIII and illustrated in Figure 8 (typical case), Figure 9 (worst case, with maximal deviation) and Figure 10, Figure 11 and Figure 12 (example of best case).

TABLE VII
COEFFICIENT OF DETERMINATION R^2

Env.	H2C	H2W	H2T	H2E	H2B
Bedroom	0.73	0.69	0.76	0.78	0.71
Living room	0.79	0.73	0.75	0.80	0.74
Office	0.81	0.77	0.78	0.79	0.74
Meeting room	0.83	0.75	0.73	0.82	0.73
Classroom	0.76	0.70	0.75	0.81	0.68
Corridor Office	0.92	0.89	0.91	0.94	0.92

TABLE VIII
VARIANCE RATIO χ

RL	H2C	H2W	H2T	H2E	H2B
Bedroom	3.7	3.2	4.2	4.5	3.5
Living room	4.8	3.7	4.0	5.1	3.8
Office	5.2	4.4	4.5	4.7	3.9
Meeting room	6.0	4.0	3.8	5.5	3.7
Classroom	4.1	3.3	4.1	5.3	3.2
Corridor Office	12.6	9.4	10.7	15.8	12.6

[7] Note that the representativeness of these test samples was verified (using KS tests) by comparing them with the training samples.

TABLE IX
RANGES OF THE PL AND THE RESIDUAL ERROR IN dB

Env.	H2C	H2W	H2T	H2E	H2B
Bedroom	1.3/0.5	5.3/3.3	1.4/0.5	3.2/1.8	3.8/1.9
Living room	1.5/0.3	4.9/2.3	1.8/0.4	3.3/1.5	3.5/1.7
Office	1.3/0.6	6.4/3.6	1.5/0.8	4.7/2.4	5.0/3.3
Meeting room	1.3/0.4	6.4/3.2	1.4/0.8	5.0/2.2	5.2/3.5
Classroom	1.6/0.3	4.0/2.3	1.6/0.3	2.6/1.4	2.7/1.6
Corridor Office	2.4/0.8	9.3/3.6	3.0/1.2	7.6/2.6	8.3/2.8

It can therefore be seen that the results obtained are satisfactory or even very satisfactory. The values of the coefficient of determination R^2 range between 0.68 and 0.94. This shows a good to very satisfactory goodness of fit. The ratio of variances is between 3.2 and 15.8, showing a significant reduction of variability. The model parameters for all the configurations studied are presented in the Appendix.

Last but not least, as expected, the range of variability is greater for NLOS RL (subject to a body masking effect), between 2.6 and 9.3 dB, see Table IX, e.g. 7.6 dB for the H2E link in corridor office (Figure 11), whereas for links that are quasi-LOS (H2C and H2T) the difference is smaller, typically between 1.3 and 3.0 dB.

2) *Cross-validation*

Cross-validation tests were carried out with separate but smaller test samples (due to long simulation times)[7]. This choice is based on the following considerations: 1. the models are based on a physical approach to the problem (notably linked to its geometry), and 2. they are average channel gain models, extracted from data from which small-scale or frequency-selective fading has been "smoothed" by frequency, small-scale (micro-positioning) and angular averaging. As a result, a fairly smooth behavior of the models as a function of the input variables is expected, so that it seems very likely that any possible overfitting problem can be detected quite easily, even with relatively modest sample sizes. The representativeness of these test samples was assessed by calculating the R^2, which in some cases deteriorated very slightly (cf. Table X).

TABLE X
COEFFICIENT OF DETERMINATION R^2

Env.	H2C	H2W	H2T	H2E	H2B
Bedroom	0.70	0.67	0.73	0.75	0.69
Living room	0.78	0.68	0.69	0.76	0.73
Office	0.78	0.73	0.78	0.78	0.68
Meeting room	0.81	0.71	0.68	0.79	0.72
Classroom	0.74	0.66	0.71	0.71	0.68
Corridor Office	0.88	0.88	0.90	0.92	0.91

TABLE XI
D_{CDF} OF KS TESTS ($D_{nm} = 0.23$)

Env.	D_{CDF}				
	H2C	H2W	H2T	H2E	H2B
Bedroom	0.10	0.09	0.10	0.09	0.05
Living room	0.10	0.14	0.09	0.09	0.10
Office	0.06	0.15	0.12	0.10	0.11
Meeting room	0.08	0.06	0.10	0.09	0.14
Classroom	0.09	0.10	0.10	0.11	0.12
Corridor Office	0.11	0.15	0.09	0.09	0.06

Recall that a Kolmogorov-Smirnov test (KS test) assesses the statistical adequacy of two samples by calculating the maximal distance between their (cumulative distribution functions (CDFs). More precisely, for each sub-sample pair, the distance D_{CDF} between both CDFs is compared with a threshold D_{nm} which depends on the size n and m of each sub-sample ($D_{nm} = 0.182$ here), in order to define the statistical representativeness according to a confidence interval α.

The KS test is successful in all cases, as the null hypothesis (i.e the two samples have the same statistic) is not rejected (as $D_{CDF} < D_{nm}$) with a confidence interval equals to $1 - \alpha$ with $\alpha = 0.01$ (a much stricter value than the commonly used value $\alpha = 0.05$) (Table XI).

V. Conclusions And Perspectives

The methodology proposed in this work, combining electromagnetic and RT simulations with measurements to assess, validate and calibrate the simulation results, has made it possible to obtain significant sample sizes. In addition, the development of experimental designs based on in-depth data collection concerning the types of environments considered (variability of room size and material characteristics) has enabled simulation campaigns of significant size to be carried out, offering a much broader and more realistic statistical representativeness than that published in the literature to date. This representative statistical variability of the "environment" parameters has, to our knowledge, never been reached in the context of WBAN communications (qualitatively and quantitatively).

Despite the complexity of the environments considered (inhomogeneity of the walls and high variability of the excursion considered for the input parameters), the parametric PL models obtained – functions of input variables ("explicative" variables) derived from the physics and geometry of the problem – made it possible to significantly reduce its random variability (i.e. its "unexplained" part), while maintaining moderate complexity.

Accordingly, this approach might be extended toward a *local* model, which would also take into account the positioning of the subject in the room (Mp and ψ), in addition to their characteristics. The results presented above lend some credibility to the success of such an extension, although considerably more complex, which is currently under development.

Finally, as indicated in the introduction, further work is also required to take into account the presence of scattering objects in rooms (furniture, etc.), as well as diffraction and diffuse scattering phenomena.

VI. Appendix

A. Models parameters

The model parameters for all the scenarios considered (i.e. (*RL*,*EC*)) are shown in Table XII. Recall that the model errors $\delta\bar{G}_c^{av}$ are all zero-mean normal r.v. of standard deviation $\sigma_{\delta\bar{G}_c^{av}}$.

Table XII
Models Parameters For Bedroom

Model Param.	Bedroom				
	H2C	**H2W**	**H2T**	**H2E**	**H2B**
α_0	$1.59\cdot10^{-5}$	$2.12\cdot10^{-8}$	$6.02\cdot10^{-6}$	$-2.12\cdot10^{-7}$	$-3.82\cdot10^{-8}$
α_1	$2.54\cdot10^{-2}$	$7.09\cdot10^{-3}$	$2.62\cdot10^{-2}$	$6.96\cdot10^{-3}$	$3.22\cdot10^{-3}$
α_2	$-1.51\cdot10^{-2}$	$5.87\cdot10^{-4}$	$2.90\cdot10^{-4}$	$-1.80\cdot10^{-3}$	$-4.60\cdot10^{-4}$
α_3	$-1.43\cdot10^{-4}$	$-7.94\cdot10^{-6}$	$-2.65\cdot10^{-5}$	$-2.08\cdot10^{-5}$	$-7.39\cdot10^{-6}$
α_4	$2.74\cdot10^{-4}$	$8.88\cdot10^{-6}$	$2.91\cdot10^{-5}$	$3.72\cdot10^{-5}$	$1.48\cdot10^{-5}$
α_{34}	$-1.20\cdot10^{-3}$	$-9.17\cdot10^{-4}$	$-3.92\cdot10^{-3}$	$-8.34\cdot10^{-4}$	$-4.52\cdot10^{-4}$
α_{35}	$1.07\cdot10^{-3}$	$5.37\cdot10^{-4}$	$2.76\cdot10^{-3}$	$6.63\cdot10^{-4}$	$3.63\cdot10^{-4}$
α_{46}	$-1.52\cdot10^{-4}$	$9.09\cdot10^{-4}$	$4.27\cdot10^{-3}$	$7.46\cdot10^{-4}$	$4.25\cdot10^{-4}$
$\sigma_{\delta\bar{G}_c^{av}}$	$5.21\cdot10^{-7}$	$7.26\cdot10^{-8}$	$1.65\cdot10^{-7}$	$6.40\cdot10^{-8}$	$3.99\cdot10^{-8}$

Table XIII
Models Parameters For Living room

Model Param.	Living room				
	H2C	**H2W**	**H2T**	**H2E**	**H2B**
α_0	$1.65\cdot10^{-5}$	$2.32\cdot10^{-7}$	$7.65\cdot10^{-6}$	$8.93\cdot10^{-9}$	$7.52\cdot10^{-8}$
α_1	$-2.67\cdot10^{-2}$	$-2.93\cdot10^{-2}$	$-7.15\cdot10^{-2}$	$-2.25\cdot10^{-3}$	$-7.43\cdot10^{-3}$
α_2	$7.75\cdot10^{-3}$	$9.73\cdot10^{-3}$	$2.36\cdot10^{-2}$	$5.97\cdot10^{-4}$	$2.07\cdot10^{-3}$
α_3	$-7.19\cdot10^{-5}$	$1.53\cdot10^{-5}$	$6.70\cdot10^{-5}$	$-6.82\cdot10^{-6}$	$-2.39\cdot10^{-7}$
α_4	$1.55\cdot10^{-4}$	$-1.13\cdot10^{-5}$	$-6.98\cdot10^{-5}$	$1.55\cdot10^{-5}$	$4.67\cdot10^{-6}$
α_{34}	$2.25\cdot10^{-3}$	$1.84\cdot10^{-3}$	$4.45\cdot10^{-3}$	$1.73\cdot10^{-4}$	$5.29\cdot10^{-4}$
α_{35}	$1.78\cdot10^{-3}$	$2.13\cdot10^{-4}$	$-2.15\cdot10^{-4}$	$2.21\cdot10^{-4}$	$3.20\cdot10^{-5}$
α_{46}	$-4.22\cdot10^{-3}$	$-2.24\cdot10^{-3}$	$-4.79\cdot10^{-3}$	$-3.27\cdot10^{-4}$	$-6.41\cdot10^{-4}$
$\sigma_{\delta\bar{G}_c^{av}}$	$3.65\cdot10^{-7}$	$5.62\cdot10^{-8}$	$1.37\cdot10^{-7}$	$4.48\cdot10^{-8}$	$3.11\cdot10^{-8}$

Table XIV
Models Parameters For Office

Model Param.	Office				
	H2C	**H2W**	**H2T**	**H2E**	**H2B**
α_0	$1.26\cdot10^{-5}$	$-4.98\cdot10^{-7}$	$5.14\cdot10^{-6}$	$-1.08\cdot10^{-6}$	$-9.60\cdot10^{-7}$
α_1	$-6.82\cdot10^{-2}$	$-8.02\cdot10^{-3}$	$-1.71\cdot10^{-2}$	$-1.27\cdot10^{-2}$	$-1.05\cdot10^{-2}$
α_2	$5.68\cdot10^{-2}$	$5.33\cdot10^{-3}$	$-9.29\cdot10^{-4}$	$1.21\cdot10^{-2}$	$1.13\cdot10^{-2}$
α_3	$3.49\cdot10^{-4}$	$3.33\cdot10^{-5}$	$2.15\cdot10^{-5}$	$6.29\cdot10^{-5}$	$5.89\cdot10^{-5}$
α_4	$-4.80\cdot10^{-5}$	$-1.01\cdot10^{-5}$	$-9.29\cdot10^{-7}$	$-1.06\cdot10^{-5}$	$-1.25\cdot10^{-5}$
α_{34}	$-3.74\cdot10^{-3}$	$4.07\cdot10^{-4}$	$4.05\cdot10^{-3}$	$-8.35\cdot10^{-4}$	$-1.09\cdot10^{-3}$
α_{35}	$1.10\cdot10^{-2}$	$-3.18\cdot10^{-4}$	$-6.14\cdot10^{-3}$	$2.40\cdot10^{-3}$	$2.65\cdot10^{-3}$
α_{46}	$-1.90\cdot10^{-3}$	$-6.96\cdot10^{-4}$	$-2.83\cdot10^{-3}$	$-4.53\cdot10^{-4}$	$-1.53\cdot10^{-4}$
$\sigma_{\delta\bar{G}_c^{av}}$	$5.26\cdot10^{-7}$	$9.78\cdot10^{-8}$	$2.68\cdot10^{-7}$	$9.27\cdot10^{-8}$	$7.04\cdot10^{-8}$

Table XV
Models Parameters For Meeting room

Model Param.	Meeting room				
	H2C	**H2W**	**H2T**	**H2E**	**H2B**
α_0	$2.16\cdot10^{-5}$	$5.06\cdot10^{-7}$	$7.00\cdot10^{-6}$	$2.03\cdot10^{-7}$	$-5.17\cdot10^{-9}$
α_1	$1.49\cdot10^{-2}$	$4.57\cdot10^{-3}$	$7.74\cdot10^{-3}$	$3.16\cdot10^{-3}$	$2.87\cdot10^{-3}$
α_2	$5.34\cdot10^{-3}$	$1.72\cdot10^{-3}$	$4.32\cdot10^{-3}$	$9.39\cdot10^{-4}$	$4.69\cdot10^{-4}$
α_3	$2.24\cdot10^{-5}$	$1.46\cdot10^{-6}$	$1.23\cdot10^{-5}$	$-7.66\cdot10^{-6}$	$-7.47\cdot10^{-6}$
α_4	$-3.76\cdot10^{-5}$	$-1.26\cdot10^{-5}$	$-3.52\cdot10^{-5}$	$6.64\cdot10^{-6}$	$9.40\cdot10^{-6}$
α_{34}	$-1.75\cdot10^{-3}$	$-3.23\cdot10^{-4}$	$-6.60\cdot10^{-4}$	$-2.39\cdot10^{-4}$	$-2.23\cdot10^{-4}$
α_{35}	$1.85\cdot10^{-3}$	$6.96\cdot10^{-5}$	$2.41\cdot10^{-4}$	$4.26\cdot10^{-4}$	$3.69\cdot10^{-4}$

α_{46}	$1.93\cdot10^{-3}$	$2.97\cdot10^{-4}$	$7.44\cdot10^{-4}$	$4.74\cdot10^{-5}$	$2.85\cdot10^{-5}$
$\sigma_{\delta\tilde{G}_c^{av}}$	$4.04\cdot10^{-7}$	$8.53\cdot10^{-8}$	$2.32\cdot10^{-7}$	$7.04\cdot10^{-8}$	$6.65\cdot10^{-8}$

TABLE XVI
MODELS PARAMETERS FOR CLASSROOM

Model Param.	Classroom				
	H2C	H2W	H2T	H2E	H2B
α_0	$1.80\cdot10^{-5}$	$6.01\cdot10^{-8}$	$5.98\cdot10^{-6}$	$4.50\cdot10^{-8}$	$1.06\cdot10^{-7}$
α_1	$-3.18\cdot10^{-3}$	$4.65\cdot10^{-4}$	$1.75\cdot10^{-3}$	$1.76\cdot10^{-3}$	$1.69\cdot10^{-3}$
α_2	$1.32\cdot10^{-2}$	$4.27\cdot10^{-3}$	$8.27\cdot10^{-3}$	$3.17\cdot10^{-4}$	$-1.75\cdot10^{-4}$
α_3	$-7.04\cdot10^{-7}$	$6.00\cdot10^{-6}$	$8.03\cdot10^{-7}$	$-2.65\cdot10^{-6}$	$-4.82\cdot10^{-6}$
α_4	$1.07\cdot10^{-4}$	$-3.51\cdot10^{-6}$	$-3.64\cdot10^{-7}$	$1.40\cdot10^{-5}$	$9.55\cdot10^{-6}$
α_{34}	$-9.67\cdot10^{-4}$	$-7.20\cdot10^{-4}$	$-1.42\cdot10^{-3}$	$-2.27\cdot10^{-4}$	$-1.50\cdot10^{-4}$
α_{35}	$3.23\cdot10^{-3}$	$1.13\cdot10^{-3}$	$2.47\cdot10^{-3}$	$2.53\cdot10^{-4}$	$1.58\cdot10^{-4}$
α_{46}	$-3.60\cdot10^{-3}$	$3.24\cdot10^{-4}$	$5.45\cdot10^{-4}$	$-9.87\cdot10^{-5}$	$-2.25\cdot10^{-5}$
$\sigma_{\delta\tilde{G}_c^{av}}$	$2.75\cdot10^{-7}$	$4.21\cdot10^{-8}$	$8.31\cdot10^{-8}$	$2.99\cdot10^{-8}$	$2.32\cdot10^{-8}$

TABLE XVII
MODELS PARAMETERS FOR OFFICE

Model Param.	Corridor Office				
	H2C	H2W	H2T	H2E	H2B
α_0	$2.07\cdot10^{-5}$	$2.31\cdot10^{-7}$	$6.36\cdot10^{-6}$	$2.87\cdot10^{-7}$	$1.17\cdot10^{-7}$
α_1	$5.13\cdot10^{-2}$	$4.43\cdot10^{-3}$	$-4.43\cdot10^{-3}$	$-4.03\cdot10^{-3}$	$-1.49\cdot10^{-3}$
α_2	$2.22\cdot10^{-3}$	$1.24\cdot10^{-3}$	$3.40\cdot10^{-3}$	$1.79\cdot10^{-3}$	$9.45\cdot10^{-4}$
α_3	$-3.20\cdot10^{-5}$	$-1.56\cdot10^{-6}$	$3.12\cdot10^{-5}$	$6.27\cdot10^{-8}$	$-7.38\cdot10^{-6}$
α_4	$7.94\cdot10^{-6}$	$-1.31\cdot10^{-6}$	$-6.49\cdot10^{-6}$	$6.49\cdot10^{-7}$	$2.84\cdot10^{-6}$
α_{34}	$-1.02\cdot10^{-3}$	$-7.83\cdot10^{-5}$	$-2.63\cdot10^{-4}$	$1.11\cdot10^{-4}$	$1.19\cdot10^{-4}$
α_{35}	$-1.73\cdot10^{-3}$	$-1.67\cdot10^{-4}$	$1.88\cdot10^{-3}$	$4.69\cdot10^{-4}$	$2.04\cdot10^{-5}$
α_{46}	$4.47\cdot10^{-4}$	$-2.24\cdot10^{-5}$	$2.23\cdot10^{-5}$	$-1.25\cdot10^{-4}$	$-7.29\cdot10^{-5}$
$\sigma_{\delta\tilde{G}_c^{av}}$	$7.03\cdot10^{-7}$	$1.11\cdot10^{-7}$	$3.03\cdot10^{-7}$	$8.37\cdot10^{-8}$	$8.00\cdot10^{-8}$

REFERENCES

[1] K. A. Michalski1 and J. R. Mosig, "Overview of the Near-Ground Propagation Mechanisms in Wireless Communication: Is the Norton Surface Wave Significant?," Reviews of Electromagnetics, Vol. I, 2022, DOI: 10.53792/roe/2022.1/21011.

[2] T. Zasowski, F. Althaus, A. Wittneben and G. Troster, "UWB for noninvasive wireless body area networks: Channel measurements and results," in *Proceedings of the IEEE Conference on Ultrawideband Systems Technology* (*UWBST'03*), pp. 285–289, November 2003.

[3] A. Fort *et al*, "Ultra-Wideband Channel Model for Communication Around the Human Body," *IEEE JSAC*, vol. 24, n° 4, Apr. 2006.

[4] A. F. Molisch *et al*, "A Comprehensive Standardized Model for Ultrawideband Propagation Channels," *IEEE Trans. Antennas Propag.*, vol. 54, no. 11, pp. 2055–2067, Nov. 2006.

[5] A. F. Molisch *et al*, "IEEE 802.15.4a channel model - final report," (*P802.15-04-0662-04-0.04a-channel-model-final-report-r1*), Oct. 2005.

[6] A. Fort et al, "An Ultra-Wideband Body Area Propagation Channel Model–From Statistics to Implementation," *IEEE Trans. MTT*, vol. 54, n°4, Apr. 2006.

[7] P. S. Hall *et al*., "Antennas and Propagation for On-Body Communication Systems," *IEEE Antennas and Propagation Mag.*, vol. 49, n° 3, June 2007.

[8] N.-G. Kang, C. Cho, S.-H. Park, E. T. Won, "Channel Models for WBANs," *IEEE 802.15 Task Group 6 Document*, Nov. 2008.

[9] C. Roblin, "Propagation channel models for BANs: an overview,"COST 2100TD(09) 760, Braunschweig, Germany, Feb. 2009.

[10] R. D'Errico and L. Ouvry, "A Statistical Model for On-Body Dynamic Channels," *International Journal of Wireless Information Networks*, Sept. 2010.

[11] M. Hirose, "StatisticalModeling of Ultrawideband Body-CentricWireless Channels Considering RoomVolume," International Journal of Antennas and Propagation, vol. 2012, Oct. 2012.

[12] FCC, "First report and order, revision of Part 15 of the Commission's rules regarding ultra-wideband transmission systems," Technical document ET Docket 98-153, FCC, April 2002.

[13] C. Roblin *et al*, "Antenna design and channel modeling in the BAN context — part II: channel," Annals of telecommunications (Springer), Special issue: "Body Area Networks applications and technologies," vol. 66, N° 3/4, Mar./Apr. 2011, pp. 157-175.

[14] Y.-F. Wei and C. Roblin, "Multislot Antenna with a Screening Backplane for UWB WBAN," International Journal of Antennas and Propagation, vol. 2012, Oct. 2012.

[15] B. Youssef and C. Roblin, "A Statistical Assessment of Anthropo-morphic Characteristics Impacts on WBAN Communications," in Proc. EuCAP, Madrid, Spain, Mar. 2022, pp. 1–5.

[16] B. Youssef and C. Roblin, "A Statistical Model for On-Body Channels in Indoor Considering Rooms Geometry and Subject Location," in Proc. EuCAP, Krakow, Poland, Apr. 2019, pp. 1–5.

[17] C. Roblin, "Representation, characterization, and modeling of ultra wide band antennas," in Ultra Wide Band Antennas, X. Begaud, Ed., New YorkUSA, Wiley, 2011, pp. 61–112.

[18] C. Roblin, "Ultra Compressed Paremetric Modelling of UWB Antenna Measurements," in Proc. EuCAP, Nice, France, Nov. 2006 pp 1–8.

[19] J. Hansen and M. Nold, "Analytic Calculation of the Power Delay Profile for Single Room Wireless LAN Environments," in Proc. Globecom '00 Conf., San Francisco, Nov. 27 – Dec. 1;2000.

[20] J. Hansen, "Analytical Calculation of Power Delay Profile and Delay Spread with Experimental Verification," IEEE Communications Letters, vol.7, no. 6, June 2003, pp. 257 - 259.

[21] M. D. McKay, R. J. Beckman, and W. J. Conover, "A comparison of three methods for se>lecting values of input variables in the analysis of output from a computer code," *Technometrics*, vol. 21, no. 2, pp. 239–245,May 1979.

[22] "French Building and Housing Code". [Online]. Available : https://www.legifrance.gouv.fr/codes/texte_lc/LEGITEXT000006074096.

[23] "Decree no. 2002-120 of January 30, 2002 on housing characteristics". [Online] Available: https://www.legifrance.gouv.fr/loda/id/JORFTEXT000000217471.

[24] UNESCO, "Norms and standards for school buildings [Online]. Available: https://unesdoc.unesco.org/ark:/48223/pf0000070131_fre.

[25] M. Lott, I. Forkel, "A Multi-Wall-and-Floor Model for Indoor Radio Propagation," *in Proc. IEEE VTS*, 53rd Vehicular Tech. Conf., Rhodes, Greece, May 2001.

[26] D. V. Giri & F.M. Tesche, "Modeling of Propagation Losses in Common Residential and Commercial Building Walls," Dept. of ECE, University of New Mexico, Aug. 2013. Internaction note IN 624.

[27] F. Sagnard, "Characterisation of materials in UWB," UWB Autumn School –GDR Waves, Valence, France, Oct. 2006.

[28] R. Wilson, "Reflection and Transmission Losses Through Common Building Materials 2.4 GHz vs 5 GHz," UltRa Lab, Univ. Southern California, Magis Network Inc, Aug. 2002.

[29] ITU-R P.2040-2, "Effects of building materials and structures on radiowave propagation above about 100 MHz," Sept. 2021.

[30] I.S. Gradshteyn and I.M. Ryzhik, Table of Integrals, Series, and Products, Seventh Edition, USA, *Academic Press – Elsevier*, 2007, §8.31 and 8.38, pp. 892-910.

[31] A. Sklar, (1959), "Fonctions de répartition à n dimensions et leurs marges"," Publ. Inst. Statist. Univ. Paris, vol. 8, pp. 229–231.

[32] "Size of premises windows". [Online]. Available: https://www.internorm.fr/actus/fenetres/.

[33] Ponomarenko-Timofeev, O. Galinina, A. Turlikov and S. Andreev, "On the Benefits of Ray-Based Modeling for Analyzing On-Body MmWave Systems," 2020 IEEE 31st Annual International Symposium on Personal, Indoor and Mobile Radio Communications, London, UK, 2020, pp. 1-6, doi: 10.1109/PIMRC48278.2020.9217339.

[34] B. Youssef and C. Roblin, "Statistical Modeling of WBAN channels in Indoor Environments Based on Measurements and Ray Tracing," *in Proc. EuCAP*, Düsseldorf,. Germany. Mar. 2021 pp. 1–5.

[35] "IT'IS Foundation Virtual Population". [Online]. Available: https://itis.swiss/virtual-population/ .